

Asteroid Size-Frequency Distribution

(The ISO Deep Asteroid Survey)

Final Report (Item 25)

21 September 2001

Contractor: TerraSystems, Inc.
2800 Woodlawn Drive, Suite 264
Honolulu, Hawai'i 96822

Contact: Dr. Edward F. Tedesco (P.I.)
(603) 659-5620 (voice)
(603) 659-2982 (fax)
etedesco@TerraSys.com

ISO Contract: NAS5-97215
Project Title: Asteroid Size-Frequency Distribution
Reporting Period: Final Report
Report Date: 21 September 2001

This is a pre-print of a paper submitted to the Astronomical Journal

Table of Contents

ABSTRACT	3
1. INTRODUCTION.....	3
2. THE ISO DEEP ASTEROID SURVEY - IDAS	4
3. ISOCAM DATA REDUCTION	6
3.1 Observation characteristics	6
3.2 Summary of data reduction	6
4. ASTEROID IDENTIFICATION	8
4.1 IDAS asteroids	8
4.2 Known asteroids associated with IDAS sources.....	9
5. SUMMARY	10
ACKNOWLEDGEMENTS	11
REFERENCES.....	12
Tables	14
Figures	18

The ISO Deep Asteroid Survey¹

Edward F. Tedesco

TerraSystems, Inc., 59 Wednesday Hill Road, Lee, New Hampshire 03824

E-mail: etedesco@terrasys.com

and

Francois-Xavier Désert

Laboratoire d'Astrophysique, Observatoire de Grenoble BP 53,

414 rue de la piscine, F-38041 Grenoble Cedex 9 France

E-mail: Francois-Xavier.Desert@obs.ujf-grenoble.fr

Keywords: minor planets, asteroids; infrared radiation — solar system

ABSTRACT

A total of six deep exposures (using AOT CAM01 with a 6" PFOV) through the ISOCAM LW10 filter (IRAS Band 1, i.e., 12 μm) were obtained on a ~ 15 arcminute square field centered on the ecliptic plane. Point sources were extracted using the technique described by Desert, et al. (1999, A&A 342, 363). Two known asteroids appear in these frames and 20 sources moving with velocities appropriate for main belt asteroids are present. Most of the asteroids detected have flux densities less than 1 mJy, i.e., between 150 and 350 times fainter than any of the asteroids observed by IRAS (Tedesco, et al., 2002a, Astron J., submitted). These data provide the first direct measurement of the 12 μm sky-plane density for asteroids on the ecliptic equator.

The median zodiacal foreground, as measured by ISOCAM during this survey, is found to be 22.1 ± 1.5 mJy per pixel, i.e., 26.2 ± 1.7 MJy/sr.

The results presented here imply that the actual number of kilometer-sized asteroids is significantly greater than previously believed and in reasonable agreement with the Statistical Asteroid Model (Tedesco, et al., 2002b, Astron J., to be submitted.).

1. INTRODUCTION

Most main belt asteroids are found between 2.2 and 3.4 AU from the Sun and at ecliptic latitudes less than 20 degrees. Except for the largest asteroids, the actual number above a given size is poorly known. For example, estimates of the number of main-belt asteroids with diameters larger than 1 km range from 3×10^4 to 1×10^7 (Farniella and Davis, 1994).

The asteroid size distribution is important because it provides constraints on models of the original size distribution of the planetesimals formed in the inner solar system and their subsequent evolution. It is also an important datum in modeling the numerical size of the population of near-Earth asteroids and accounting for their evolution from the main belt into Earth-orbit-crossing orbits.

¹Based on observations with the Infrared Space Observatory (ISO), an ESA project with instruments funded by ESA Member States (especially the PI countries: France, Germany, the Netherlands, and the United Kingdom) with the participation of ISAS and NASA.

A typical 1 km main belt asteroid has a V magnitude between 21 and 23. It would be a straightforward program to survey, at visible wavelengths, all asteroids in given regions of the sky brighter than this limit. However, because, for any given distance, visual surveys are biased in favor of discovering higher-albedo asteroids, magnitude data alone cannot be used to accurately derive asteroid diameters. This is because the absolute brightness of an asteroid depends upon its cross section and albedo, and asteroid albedos span a range of at least a factor of 25 (0.02 to >0.5). Moreover, there may be systematic trends of albedo with size (Tedesco, 1994).

Observing thermal emission permits us to obtain an accurate distribution of asteroid diameters because, unlike the linear dependence with albedo at visual wavelengths, the infrared flux is only weakly dependant on the geometric albedo. For example, on 26 March 2001 the 100 km main belt asteroid 50 Virginia was at a solar elongation of 110° , a typical elongation for space-based infrared observations. Virginia's visual magnitude at this time, given its SIMPS (Tedesco, et al., 2002a) diameter of 99.82 km, would be 14.9 if its visual geometric albedo were 0.02 and 18.4 if its visual geometric albedo were 0.50, a difference of 3.5 mag. The $12.0\ \mu\text{m}$ magnitudes under these same conditions, would be 2.16 and 2.46, respectively, or a difference of only 0.3 mag. Furthermore, the lower albedo actually results in a slightly higher $12.0\ \mu\text{m}$ brightness because in this case the asteroid's temperature would be higher. Thus, an IR survey is slightly biased in favor of discovering lower-albedo asteroids.

To date there have been three space-based infrared surveys in which asteroids have been incidentally observed: The Infrared Astronomical Satellite (IRAS), the Midcourse Space Experiment (MSX, Mill et al., 1994), and the Infrared Space Observatory (ISO) spacecraft, reported on here. For a description of the ISO mission see Kessler et al. (1996) and for details on the ISOCAM instrument see Cesarsky et al. (1996).

Results on IRAS asteroids are given in Tedesco et al. (1992, 2002a) and those on asteroids observed by MSX by Tedesco et al. (2002c).

The IRAS asteroid survey is severely incomplete at low flux levels, *i.e.*, below about 1 Jy, because IRAS could only detect an asteroid in its survey mode if a known orbit was available. Thus, although IRAS observed at infrared wavelengths, it was limited by the (albedo-biased) visual surveys in which asteroids are discovered and from which data their orbits are calculated. (IRAS knowingly discovered no main-belt asteroids due primarily to the poor spatial resolution of its detectors.)

IRAS and MSX serendipitously observed numerous asteroids in the course of their nominal missions. However, due to the way in which their observations were conducted, only asteroids with known orbits were identified with the infrared sources these spacecraft detected. IRAS observed ~95% of the sky and MSX about 10%. Although the faintest asteroids detected in these surveys have flux densities of about 150 mJy, they are in no way complete to this flux level. The ISO asteroid "survey" (discussed below) observed about 0.125 sq deg of sky to a completeness limit of ~0.6 mJy.

2. THE ISO DEEP ASTEROID SURVEY - IDAS

The goal of this survey was to cover the maximum area of sky to the faintest flux limit possible under the constraints imposed by the zodiacal background and the

available observing time. The field was selected to be in the ecliptic plane, near the upper limit of the ISO solar elongation constraint (i.e., near 106°), and located west of the Sun (to facilitate ground-based follow-up). In addition, the field was chosen to lie far from the Galactic plane and to contain no known IRAS sources or bright stars. The sensor used was ISO's AOT CAM01 with a 6-arcsecond PFOV and using the ISOCAM LW10 filter (IRAS Band 1, i.e., $12\ \mu\text{m}$).

Asteroids move and their flux may vary appreciably on time scales as short as minutes. Consequently, the exposure time was chosen to freeze asteroid motion on each sub-map, where a sub-map is a three-by-three arcminute area (the size of the ISOCAM array) in which each point was observed three times. Each sub-map consisted of a 30 second exposure sequence² at a fixed position followed by a step of one arcminute in ecliptic longitude or latitude where the exposure sequence was repeated and ending with another one arcminute step in ecliptic longitude or latitude where the exposure sequence was again repeated. The total time spent doing each point in a sub-map was 90 seconds. Because the apparent rate of motion for main belt asteroids (MBAs), under the observing geometry described above, is between 0 and 60 arcseconds per hour, the maximum angular distance moved during the time required to obtain a sub-map is less than 1.5-arcsecond. However, each sub-map was sampled three times to create the complete map, and the times between successive sub-maps varied from 30 sec to 870 sec. Thus, the maximum distance a main belt asteroid would move between samples of a given point in the map is 14.5-arcseconds.

Figure 1 is a schematic diagram of the map coverage. Each box is one arcminute on a side with North up and East to the right. The raster began with the 3'x3' array located in the NE corner of the map, as indicated by the heavy lines around the nine cells in the upper right of the figure. One exposure sequence was made at this position and then the array was moved one arcminute (cell) west. Seventeen exposure sequences were made along a line of constant ecliptic latitude. This brought the array to the end of the first row. At this point, it stepped South one arcminute, made an exposure sequence at this position, and then made 16 one arcminute steps to the East to complete the second row. This process was then repeated until the center of the array had scanned 17 rows.

See the movie for an animated version of this figure speeded up by a factor of about 60. As can be seen from the movie, or the numbers in the figure, each cell around the outer one arcminute of the map received no more than three exposure sequences and those in the one-arcminute border interior to this region no more than 6. All other cells in the map received 9 exposure sequences for a total of 180 seconds each. We refer to the region with 9 exposure sequences as the region of complete coverage.

The 15x15 raster map was obtained in the same way but using 15, instead of 17 steps. The complete coverage area is 15 sq arcminutes for the maps obtained with the 17x17 raster and 13 sq arcminutes for those obtained with the 15x15 raster.

Two maps as described above were made in June 1996 and another four in June 1997. A total of 13.64 hours was expended in obtaining the observations presented

² A "clean" was performed at the start of each map. This flashed the array to remove the memory of the previous observation and required about 240 seconds. Next 25 stabilization frames were taken. The actual observations consisted of four 5-sec exposures at each point in the raster, plus an average of ten seconds to step to the next raster position.

herein. Maps 1, 2, 5, and 6 required 2.44 hours per map, while maps 3 and 4 had available 1.94 hours each. A consequence of the decision to keep the exposure per map point constant over all six maps was that maps 3 and 4 cover less area.

The intention was to have maps 3 and 4 (the time for which was granted under a Supplemental Observing Request) made at least 36 hours after the end of the previous map pair. However, they were scheduled less than 12 hours after completion of the previous map and by the time the observing schedule was issued it was too late to reschedule them.

The sample consists of six data sets that are now in the public domain³ labeled as Target Dedicated Time (TDT) numbers: 21103003, 21103004, 57200101, 57200102, 57200407, and 57200408 (corresponding, respectively, to map numbers 1, 2, 3, 4, 5, and 6 in Table 1). Thus, they were taken in pairs during two 24-hour ISO orbits (the first 3 digits in the TDT) separated by approximately one year, on 15 June 1996 and 10 June 1997 (i.e., on Julian days 2450249 and 2450609, respectively).

Figure 2 shows the six images obtained after processing using the technique of Desert, et al. (1999), which is further described in Sec. 3. Figure 3 shows all point sources with $\text{SNR} \geq 3.0$ extracted from the ISOCAM maps shown in Figure 2. Squares outline the areas sampled nine times. The point size is proportional to the flux density, which ranges from 0.3 to 12.2 mJy

3. ISOCAM DATA REDUCTION

3.1 Observation characteristics

A typical dataset consists of 1800 readouts, each with 5.1 seconds of integration, through the ISOCAM LW10 filter centered at 12 μm with a bandpass very similar to the IRAS 12 μm band. The lens wheel was on the LGe6 position providing a ratio of 6 arcseconds per detector pixel (which is also close to the FWHM of the Airy pattern of ISO). The camera detector consists of 32 by 32 pixels, with one column (number 24, disconnected before launch) missing, providing a 3.2 by 3.2 arcmin instantaneous field of view. The total survey area was covered by making a raster with ISO at positions on a 17 by 17 grid with 60 arcsecond (10 pixel) steps and 60 arcsecond line separation. Each position was observed for four readouts, i.e., 20 seconds of integration time. With the survey redundancy (a factor 9), the total integration time per sky pixel is about 3 minutes. The median zodiacal foreground, as measured by ISOCAM during this survey, is found to be 22.1 ± 1.5 mJy per pixel, i.e., 26.2 ± 1.7 MJy/sr (the error bar being the dispersion among the six surveys of the same area).

3.2 Summary of data reduction

The raw data consists of a cube (CISP files) of detector readouts (one every 36 CAM time units i.e., 5.1 seconds) and an ISO pointing history (IIPH) file. The detailed data reduction procedure is described by Désert et al. (1999). Here we give a summary along with the specific parameters that were used for the present datasets. First cosmic

³ <http://www.iso.vilspa.esa.es/>

rays are removed by a time line analysis of each pixel. Long duration glitches are also removed and a transient correction applied, using the method described by Coulais and Abergel (2000).

The data timeline is then analyzed with a “triple-beam” linear algorithm that basically finds, for each camera pixel, the difference between the signal at one raster position and the average of the 2 adjacent position signals. The dispersion of this difference for different raster positions indicate the true pixel noise of the measurements, because, most of the time, it is uncontaminated by sources. Badly behaved pixel values (due to glitches and bad triple-beam X^2) are discarded by an adapted sigma clipping. We project the difference and dispersion on a final sky map, using neighbor pixel approximation, with a 2-arcsecond pixel size. A redundancy number is also obtained this way. The projection is done by coadding with an optimal weighing and a first order array distortion correction. We used the associations with the USNO optical catalog (version A2.0 - Monet et al., 1998)⁴ to deduce the offset positions (up to 7-arcseconds in both directions) to apply to each dataset map (because of the so-called lens filter wheel jitter).

The final map is then searched for point sources in a selected area where the redundancy is two or more. As explained by Désert et al. (1999), we iterate an algorithm where a candidate source (found with a top hat wavelet) is fit with a 9-arcsecond FWHM two-dimensional Gaussian (for the position and intensity) and the fit is removed. This algorithm allows measuring source fluxes near undefined pixels without underestimating the flux (as aperture photometry would do). The noise in the flux measurement is deduced from the noise map and the Gaussian least-square fitting algorithm. The absolute fluxes were deduced using the nominal ISOCAM internal unit to mJy conversion factor (*i.e.*, by assuming that the factor has not changed with respect to pre-flight expectancy), and by applying a correction factor (1.52) to go from our fitted Gaussian beam flux to total point-spread-function integrated flux.

In Table 2⁵, we give the complete catalog of (527) sources that were detected at the $\geq 3 \sigma$ level in any of the six maps. Column (1) is an identification number; columns (2) and (3) the J2000 RA and Dec; column (4) the flux density in band LW10, (5) the one-sigma uncertainty in the flux density; (6) the signal-to-noise ratio; (7), (8), and (9) are quality flags; (10) the Julian Date of the observation (an average of the, up to, nine measurements on each point source that are available); (11) a confusion flag; and (12) a code indicating whether the source was in the multiply-sampled region. Columns (13) through (19) provide data on sources found within 6-arcseconds of a USNO-A2.0 catalog (Monet et al., 1998) visible source (as reduced by CDS-VizieR, <http://cdsweb.u-strasbg.fr/CDS.html>). Column (13) gives the red magnitude from the USNO-A2.0 catalog; column (14) the name from the USNO-A2.0 catalog; (15) the number of USNO-A2.0 sources associated with the ISO source; (16) the number from the USNO-A2.0 catalog; (17) the distance from the USNO-A2.0 catalog source (95% are within 4-arcseconds); and (18) and (19) the distances in RA and Dec, respectively, from the USNO-A2.0 catalog source, rounded to the nearest arcsecond.

⁴ As reduced by CDS-VizieR, <http://cdsweb.u-strasbg.fr/CDS.html>

⁵ Table 2 is presented in its entirety in the electric edition of the Astronomical Journal.

A catalog of 63 inertial sources is given in Table 3. These are sources from Table 2 that are seen at the same position in at least two maps. An average flux, ranging from 0.34 to 10.8 mJy, and error is given along with the USNO-A2.0 catalog association. Some well-detected sources have no optical counterparts. These are probably external galaxies or very slow-moving asteroids.

The complete (i.e., multiply observed) survey area is 225 arcmin^{-2} (0.0625 deg^{-2}). The densities of stars and galaxies (assuming all non-USNO-A2.0 sources are galaxies), respectively, are found to be 0.072 ± 0.017 and $0.045 \pm 0.013 \text{ arcmin}^{-2}$, for 12 μm flux densities greater than 0.6 mJy (a value close to the 4σ level where σ is the median flux error in the complete area for one dataset).

4. ASTEROID IDENTIFICATION

4.1 IDAS asteroids

Moving sources were searched for in those areas observed in common within a day of each other. Twenty objects were found to move significantly (i.e., by more than 6-arcseconds over a period \geq two hours).

Because asteroids are moving sources, the technique described in Sec. 3.2 for obtaining the flux from coadded images underestimates their flux. Thus, we derived a rate-of-motion dependent correction factor (FDCor) by offsetting the inertial sources by various amounts to simulate their motion and then performing the photometry as normally on the coadded map. This resulted in smaller flux values as a function of the amount offset, to which we fit a second order polynomial (shown in Figure 7), viz.,

$$\text{FDCor} = 1.001 - 0.0034*x + 0.0160*x^2, \quad (1)$$

where $x = \text{RT} \cdot 30 \cdot \text{Rate}$; and $\text{RT} = 17$ (for a 17 by 17 raster) or 15 (for a 15 by 15 raster), 30 is the time per sample, and Rate is the apparent rate of motion in arcsec per revisit interval.

Table 2 contains the uncorrected flux densities and Table 4, which presents the data on the 20 sources identified as being asteroids on the basis of forming tracks with two or more sightings, gives FDCor and the corrected flux densities, ranging from 0.43 to 5.7 mJy, for each sighting.

All of the identified asteroids have $\text{SNR} > 4$. The 1996 field contains four tracks in which at least one sighting has a flux density (FD) > 1 mJy, and the 1997 field contains six such tracks. Each field contains ten tracks, at least one of which has $\text{FD} > 0.6$ mJy, the $4\text{-}\sigma$ completeness limit.

Combining the results from the two fields gives 5 ± 1 probable asteroids with $\text{FD} > 1$ mJy and 10 ± 1 with $\text{FD} > 0.6$ mJy.

Normalizing these results, gives 80 ± 16 asteroids with $\text{FD} > 1$ mJy per sq deg at the ecliptic plane, i.e., with diameters greater than about 1.4 km at mid-belt, and 160 ± 16 with $\text{FD} > 0.6$ mJy per sq deg (diameters greater than about 1.1 km at mid-belt).

Singletons (i.e., a source detected only once) with flux densities above 0.6 mJy may also be present in these fields but they cannot be unambiguously identified using these data alone.

4.2 Known asteroids associated with IDAS sources

We associated two asteroids found in the 1996 field with known asteroids. Details on these sources are given in Table 5, where column (1) gives, as two rows per observation, the IDAS asteroid number assigned in Table 4 in the first row and the associated asteroid's designation in the second, column (2) gives the IDAS source number from Table 2, columns (3) and (4) give, respectively, the observed RA and Dec in the first row and the predicted RA and Dec, obtained using the Horizons software (Giorgini et al., 1996)⁶, in the second row, columns (5) and (6) the observed corrected flux density and SNR, respectively, and column (7) the UTC of the observation. Of the ten probable asteroids identified in this field, those associated with 1999 AQ23 and 17971 1999 JZ50 are the brightest. The predicted V-band magnitudes of these two asteroids at the time of the ISO observations were 18.2 and 18.1, respectively. This means that 80% of the asteroids in the 1996 field have $V > 18$ and, for those with low albedos (0.02), the maximum V is about 25.

Figure 6 shows the observed ISOCentric positions for sources 3 and 1008 (1999 AQ23) and sources 4 and 1003 (17971 1999 JZ50) from the 1996 ISOCAM map, together with the ISOCentric positions for the two known asteroids. According to the Horizons documentation: "The database is updated almost daily with new objects and orbit solutions. Comet and asteroid orbits are integrated from initial conditions stored in the JPL-maintained DASTCOM database⁷." Due to the ephemeral nature of these orbital elements, we present, in Table 6, those used in the analysis described here.

The ISOCAM coordinates, for the mean time of the extracted sources, are plotted in Figure 6 as triangles. Because the asteroid position is the mean from detections obtained over the ~18 minutes required to map an inertial point on the sky, the predicted positions are shown as a series of 19 positions at one-minute intervals centered on the mid-time of the local map. The small squares centered on the predicted position trails are 6" on a side, the size of an ISOCAM pixel used in this experiment, while the figure is ~3' on a side, the size of the ISOCAM array.

1999 AQ23 moved a distance equivalent to the size of a pixel during the time required to complete the raster scan of its position, while 17971 1999 JZ50 moved about twice this distance. For the numbered asteroid, 17971 1999 JZ50, the difference between the observed ISOCAM positions and the predicted ephemeris positions are 2.8" and 0.6". For the unnumbered asteroid 1999 AQ23, the observed positions lead⁸ the predicted positions by about 11" (or 34 minutes in time).

As noted in Sec 3.2, the astrometric accuracy of the IDAS positions is better than 4" for 95% of the sources associating with USNO-A2.0 sources. The accuracy for moving sources is undoubtedly less, but probably not by a factor of two to three. The formal accuracy of the asteroids' predicted positions is less than 1" (based upon output from

⁶ The "HORIZONS (<http://ssd.jpl.nasa.gov/horizons.html>) On-Line Ephemeris System" was created and is maintained by the Solar System Dynamics Group, Jet Propulsion Laboratory.

⁷ ftp://ssd.jpl.nasa.gov/pub/ssd/Horizons_doc.ps - Version 2.80 June 14, 2000.

⁸ The lead-time is the difference between the time the known asteroid is closest to the position of the ISO source minus the time of the ISO observation of that source. The track of 1999 AQ23, in ISOCentric coordinates, passes less than 1" from the observed positions.

the Lowell Observatory Asteroid Ephemeris (ASTEPH) Version 1.5 at <http://asteroid.lowell.edu/cgi-bin/koehn/asteph> run on 18 September 2001).

In spite of the relatively poor agreement in position for 1999 AQ23 we nevertheless present the albedos and diameters for both 1999 AQ23 and 17971 1999 JZ50 under the assumption that they are associated with the ISO sources indicated.

The results are presented in Table 7, where column (1) identifies the asteroid; columns (2) through (5) give the absolute visual magnitude, H , heliocentric distance, H Dist, geocentric distance, G Dist, and solar phase angle, Phase, from the Horizons ephemerides for the mid-time of the ISO observations; column (6) the corrected observed mean ISO LW10 band (\sim IRAS) 12 μ m flux density and its uncertainty; columns (7) and (8) the computed diameter and geometric albedo using the Standard Thermal Model (STM – Lebofsky et al., 1986), D-STM and p_H -STM, respectively; and columns (9) and (10) the computed diameter and geometric albedo using the Near-Earth Asteroid Thermal Model (NEATM – Harris, 1998), D-NEATM and p_H -NEATM, respectively.

The results from the photometry are ambiguous. Using the given values for H and the infrared fluxes, the derived geometric albedos, from either the STM or NEATM thermal model, are either unphysical (\sim 0.9) or implausible (\sim 0.65 to 0.71).

Physically plausible albedos can be obtained, e.g., by assuming that H for each of these asteroids is 1.0 mag higher than that published, or that H is 0.5 magnitude larger and the 12 μ m flux density is 50% higher than reported here, etc. (see Table 7). Changes of this magnitude for H are not uncommon (see Tedesco, 2002a). And a 50% underestimate of the ISO flux density is also quite possible. Furthermore, both of these asteroids are located in the inner part of the asteroid belt where, at least for asteroids with diameters greater than \sim 60 km, low albedo asteroids make up less than 10% of the population (Gradie and Tedesco, 1982). However, other than ruling out low albedos for these asteroids (because for these values of H and an albedo of 0.02 the predicted infrared flux densities range from 200 to 440 mJy, two orders of magnitude higher than observed) an accurate albedo cannot be determined.

5. SUMMARY

There are about 160 asteroids per sq deg at the ecliptic plane above the ISOCAM LW10 band (*i.e.*, IRAS Band 1, 12 μ m) detection threshold of about 0.6 mJy. This corresponds to diameters greater than about 1.1 km at mid-belt. For the fields observed in this experiment the faintest asteroid source extracted has a flux density of 0.432 ± 0.085 mJy and SNR = 4.3.

To put these results in perspective, note that IRAS' limiting sensitivity was about 150 mJy at 12 μ m whereas most of the asteroids detected by ISO are between 150 and 350 times fainter.

The Statistical Asteroid Model (Tedesco et al. 2002b) was run twice on a four sq. deg field centered on the ISO field, once for the epoch of osculation of the model's orbital elements (14 Oct 1998) and a second time (yielding the results in parentheses below) for the date of the June 1997 ISO observations.

A total of 1,063 (1,638), of the approximately two million asteroids in the Statistical Asteroid Model, were present in this four sq. deg field. Of these, 673 (852) had

predicted IRAS 12 μm flux densities greater than 0.6 mJy. Thus, the model gives 180 ± 20 asteroids per square degree with 12 μm flux densities greater than 0.6 mJy, in reasonable agreement with the ISO results reported here.

The Statistical Asteroid Model result is actually a lower limit because the model does not yet include the NEAs or asteroids beyond the Hilda group. More importantly, however, is the fact that it terminates abruptly at a diameter of 1 km. If smaller asteroids were included some of these would have 12 μm flux densities greater than 0.6 mJy if they were close to the Earth. Nevertheless, the ISO data imply that the actual number of kilometer-sized asteroids is in reasonable agreement with the Statistical Asteroid Model.

SIRTF's imagers will have $\sim 5' \times 5'$ FOV arrays with 1.2" pixels and sensitivities of ~ 0.015 mJy at 8 μm and ~ 0.37 mJy at 24 μm , about an order of magnitude more sensitive than the IDAS limit. The results presented here demonstrate that significant numbers of asteroids will be present in virtually all deep exposures taken near the ecliptic plane. Using the extreme size-frequency distributions and the IDAS asteroid sky-plane density implies that there will be between 3 and 30 asteroids in each limiting sensitivity SIRTf image. See [Tedesco et al. \(2002b\)](#) for additional discussion on this issue.

Unfortunately, in spite of the high quality of the ISO data, little can be said regarding the diameters (and nothing regarding the albedos) of the unknown asteroids detected. This is because their orbits, and hence distances and phase angles, are unknown and cannot be reliably computed from the ISO positions alone. Reliable diameter determinations for these ISO asteroids will have to await their discovery. And, with V mags probably fainter than 22 for most, this is unlikely to happen in the near future.

In order to fully exploit such space-based infrared data, orbital elements of the asteroids must be known. If albedos are to be obtained, then visual wavelength observations are required as well. The minimum requirements for obtaining asteroid diameters in the absence of supporting ground-based observations is that the space-based data must sample the asteroid's thermal spectrum at a minimum of three wavelengths bracketing the peak emission and be taken at appropriate intervals and with astrometric accuracies sufficient to allow computation of an approximate orbit.

ACKNOWLEDGEMENTS

ET gratefully acknowledges the support provided by Mary Ellen Barba, Ken Ganga, George Helou, Linda Hermans, Deborah Levine, Rosanne Scholley, Nancy Silbermann, Dave Van Buren, and Ann Wehrle in the planning, acquisition, and preliminary data reduction of the observations upon which this study was based. Thomas Mueller provided valuable input regarding associating ISO sources with known asteroids and directed ET to the Horizons system.

NASA's Astrophysics Data Program supported ET's portion of the work reported herein.

REFERENCES

- Cesarsky, C.J., and 65 others. 1996, *A&A*, **315**, L32-L37.
- Coulais, A., and Abergel, A. 2000, *A&A Supp. Ser.*, **141**, 533
- Désert, F.-X., Puget, J.-L., Clements, D. L., Pérault, M., Abergel, A., Bernard, J.-P., & Cesarsky, C.J. 1999, *A&A*, **342**, 363-377.
- Farinella, P.; Davis, D. R. 1994, Abstracts of the 25th Lunar and Planetary Science Conference, p 365.
- Giorgini, J.D., Yeomans, D.K., Chamberlin, A.B., Chodas, P.W., Jacobson, R.A., Keesey, M.S., Lieske, J.H., Ostro, S.J., Standish, E.M., Wimberly, R.N. 1996, *BAAS*, **28**, 1158.
- Gradie, J.C. & Tedesco, E.F. 1982, *Science* 216, 1405.
- Harris, A.W. 1998, *Icarus* **131**, 291.
- IRAS Catalogs and Atlases, Version 2: Explanatory Supplement. 1988, ed. C.A. Beichman, G. Neugebauer, H.J. Habing, P.E. Clegg and T.J. Chester, NASA Ref. Publ., 1190, Washington, DC: GPO.
- IRAS Minor Planet Survey⁹ 1992, ed. E.F. Tedesco, Phillips Laboratory Technical Report No. PL-TR-92-2049. Hanscom Air Force Base, MA.
- Kessler, M. F., et al. 1996, *A&A*, **315**, L27-L31
- Lebofsky, L.A., Sykes, M.V., Tedesco, E.F., Veeder, G.J., Matson, D.L., Brown, R.H., Gradie, J.C., Feierberg, M.A., Rudy, R.J. 1986, *Icarus*, **68**, 239 – 251.
- Mill, J. D., et al. 1994, *J. Spacecraft and Rockets* **31**, 900-907.

Monet et al., 1998, <http://ftp.nofs.navy.mil/projects/pmm/catalogs.html>

Tedesco, E.F. 1994, In *Asteroids, Comets, Meteors 1993*, ed. A. Milani, M. DiMartino, & A. Cellino (Dordrecht: Kluwer), 55 – 74.

Tedesco, E.F., Noah, P.V., Noah, M. & Price, S.D. 2002a, AJ, submitted.

Tedesco, E.F., Cellino, A. & Zappalà, V. 2002b, AJ, to be submitted.

Tedesco, E.F., Egan, M.P. & Price, S.D. 2002c, AJ, to be submitted.

⁹ Available from S.D. Price; Space Vehicles Directorate, Air Force Research Laboratory, 29 Randolph Road; Hanscom AFB, MA 01731-3010 E-mail: Steve.Price@hanscom.af.mil

Tables

Table 1. Map Field Centers

Map	RA J2000	Dec J2000	Raster	Ecliptic Longitude	Ecliptic Latitude
				2000 Equinox	
1	22:08:38.6	-08:34:10.4	17x17	338.000000	0.002471
2	22:08:42.5	-08:33:52.1	17x17	338.016800	0.001180
3	22:08:38.6	-08:34:10.4	15x15	338.000000	0.002471
4	22:08:41.6	-08:33:56.4	15x15	338.012900	0.001483
5	22:08:38.6	-08:34:10.4	17x17	338.000000	0.002471
6	22:08:42.5	-08:33:52.1	17x17	338.016800	0.001180

Table 2. All Point Sources Extracted From the Six IDAS Maps

This table is available only as a machine-readable table in the on-line electronic edition.

Table 3. IDAS Field Inertial Point Sources

ID	RA	Dec	FD	σ	SNR	R	USNO Name	Associations
0	339.502145	-8.506749	407	67	6.0			146; 8096
1	339.527498	-8.568980	849	52	16.2	18.9	0750-21270670	79; 1017; 4008; 8037; 9022
2	339.532663	-8.578120	450	45	10.0	13.3	0750-21270745	115; 1085; 4034; 8103; 9069
3	339.535786	-8.595465	479	59	8.2	13.5	0750-21270820	103; 1099; 4169; 8034
4	339.540586	-8.536923	1499	44	33.9			17; 1007; 4003; 8008; 9006
5	339.561057	-8.471207	1254	62	20.1	17.5	0750-21271301	14; 1023; 4007; 5069; 8009; 9009
6	339.580975	-8.517697	565	72	7.9			1270; 8152
7	339.587977	-8.503622	885	42	21.0	14.7	0750-21271831	32; 1056; 4017; 5020; 8019; 9044
8	339.590961	-8.636819	604	40	15.1	13.7	0750-21271877	36; 1045; 4048; 5104; 8075; 9034
9	339.592123	-8.482400	536	51	10.5			143; 1132; 9274
10	339.592687	-8.443355	747	119	6.3			76; 4011
11	339.596250	-8.511510	663	42	15.7			109; 1071; 4056; 5031; 8191; 9120
12	339.598123	-8.477542	4867	86	56.3	10.6	0750-21272024	1; 1000; 4001; 5001; 9001
13	339.600250	-8.668321	637	43	14.8	19.1	0750-21272064	44; 1069; 4021; 8048; 9063
14	339.603519	-8.465211	580	63	9.3			241; 5041; 8047
15	339.611103	-8.559631	429	56	7.7			1125; 8253; 9107
16	339.615798	-8.662995	416	42	10.0			215; 1169; 5198; 8146; 9087
17	339.625113	-8.436006	1342	55	24.5	16.2	0750-21272521	15; 1013; 4010; 5009; 8017; 9028
18	339.627154	-8.462892	1659	50	33.5	11.5	0750-21272547	7; 1006; 4002; 5010; 8007; 9008
19	339.628997	-8.423933	564	91	6.2			1080; 8044; 9142;
20	339.641625	-8.649331	623	45	13.8			134; 1053; 4080; 5025; 8023; 9098
21	339.648022	-8.541135	1373	47	29.2			13; 1011; 4091; 5007; 8015; 9012
22	339.651048	-8.605006	603	46	13.1			55; 4149; 5126; 8058; 9054
23	339.655479	-8.567884	417	65	6.4			236; 5219
24	339.656071	-8.591558	1082	45	24.1	12.8	0750-21273104	21; 1018; 4009; 5019; 8012; 9018
25	339.661912	-8.574583	384	74	5.2	18.8	0750-21273204	1191; 4131
26	339.663695	-8.651154	601	42	14.4	18.9	0750-21273242	125; 1059; 4038; 5076; 9104
27	339.664282	-8.732838	834	111	7.5	18.3	0750-21273245	123; 1026; 8067
28	339.668283	-8.518580	510	40	12.7	14.7	0750-21273317	136; 1121; 4170; 5046; 8073; 9139
29	339.671654	-8.515432	523	44	11.9			114; 1118; 4062; 8107; 9047
30	339.676826	-8.709590	410	70	5.9			131; 8192; 9072
31	339.681931	-8.445261	441	45	9.8	18.6	0750-21273599	185; 1057; 8072; 9092
32	339.682437	-8.450058	497	46	10.8	19.0	0750-21273607	180; 1117; 4077; 5165; 8199; 9058
33	339.684090	-8.442555	869	44	19.6	18.6	0750-21273647	81; 1038; 4012; 5030; 8022; 9067
34	339.688585	-8.492524	442	41	10.7			130; 1065; 5111; 8197; 9176
35	339.697056	-8.604695	508	47	10.9	19.7	0750-21273857	135; 1179; 8027; 9284
36	339.699698	-8.564683	1020	37	27.4	12.8	0750-21273912	18; 1029; 4015; 5008; 8011; 9020
37	339.702035	-8.602145	406	79	5.1			1184; 4207
38	339.704640	-8.466331	2166	48	45.4	18.5	0750-21274005	6; 1004; 4004; 5005; 8006; 9002
39	339.704964	-8.614536	340	72	4.7			1277; 4078
40	339.705753	-8.679018	520	54	9.6			51; 1167; 5058; 8095
41	339.707689	-8.528508	465	59	7.9			4033; 5150; 8134
42	339.707062	-8.583767	378	60	6.3			217; 8082; 9153
43	339.708279	-8.563930	473	65	7.3			1164; 8261
44	339.711638	-8.711600	1928	181	10.7	16.4	0750-21274141	19; 8030; 9014
45	339.711796	-8.686091	3937	69	56.7			2; 1002; 4000; 5000; 8000
46	339.714394	-8.455913	464	50	9.2	15.5	0750-21274181	1233; 5191; 8126; 9324;
47	339.719062	-8.596113	964	45	21.2	12.2	0750-21274288	30; 1022; 4036; 5016; 8032; 9026
48	339.720638	-8.645489	450	65	6.9	13.6	0750-21274307	261; 8104
49	339.730426	-8.432215	1212	62	19.6	18.6	0750-21274495	12; 1014; 4006; 5011; 9019;
50	339.736522	-8.488266	679	44	15.6			41; 1046; 4023; 5088; 8088; 9042
51	339.739081	-8.684950	10822	179	60.6	99.9	0750-21274627	0; 1001; 9000
52	339.752527	-8.528036	416	51	8.2			1194; 8215; 9196
53	339.757206	-8.534375	424	70	6.1			5122; 8092
54	339.761885	-8.680850	655	68	9.7			50; 1051; 8021; 9048
55	339.761725	-8.573803	636	42	15.0	17.8	0750-21275058	64; 1104; 4143; 5054; 8052; 9032
56	339.770798	-8.684376	1073	112	9.6			22; 1027; 9017
57	339.774642	-8.485023	3313	107	31.0	16.8	0750-21275320	9; 1009; 5003; 9003;
58	339.784544	-8.659310	666	52	12.9			45; 1047; 5029; 8071; 9073
59	339.790028	-8.621748	620	64	9.6			152; 9103
60	339.790029	-8.623324	479	58	8.2			1239; 5036; 8155
61	339.810757	-8.539094	2225	92	24.2	13.5	0750-21275982	1005; 5017; 9007
62	339.826604	-8.624449	766	69	11.1	18.3	0750-21276278	1019; 9039

Table 4. IDAS Asteroid Sightings

Ast	ID	RA	Dec	SNR	Q1	Q2	Q3	JD -2450000	C	FDCor	CorFD	RT
1	3	339.575977	-8.577812	25.1	1	1	4	249.79034	1	1.115	3926	17
1	1008	339.588994	-8.580972	17.2	3	4	4	249.89243	1	1.115	4225	17
2	4	339.647069	-8.463253	22.0	0	4	4	249.78111	1	1.481	5580	17
2	1003	339.672558	-8.454937	24.3	0	4	4	249.88291	1	1.481	5559	17
3	5	339.595198	-8.558890	14.8	3	4	4	249.78781	1	1.034	3111	17
3	1015	339.596613	-8.551524	13.3	2	2	4	249.89117	1	1.034	1997	17
4	35	339.754592	-8.639367	6.6	4	4	4	249.77823	1	1.127	801	17
4	1139	339.768698	-8.638212	4.0	3	3	1	249.88102	1	1.127	542	17
5	43	339.700352	-8.499148	6.3	4	4	4	249.77819	1	1.092	841	17
5	1096	339.712344	-8.497636	6.1	4	4	4	249.88087	1	1.092	597	17
6	55	339.651395	-8.604998	7.4	4	4	4	249.78502	1	2.836	2022	17
6	1184	339.702285	-8.602760	4.1	4	4	1	249.88479	1	2.836	1231	17
7	85	339.715214	-8.523705	4.5	4	4	1	249.77796	1	1.988	974	17
7	1194	339.752778	-8.528283	5.4	4	4	4	249.87869	1	1.988	908	17
8	94	339.630016	-8.415515	4.5	0	4	1	249.78104	0	1.008	781	17
8	1043	339.631924	-8.418823	4.9	0	4	1	249.88402	0	1.008	857	17
9	111	339.634837	-8.593815	5.0	4	4	3	249.78622	1	1.336	665	17
9	1063	339.656464	-8.587599	4.8	4	4	1	249.88802	1	1.336	698	17
10	230	339.647725	-8.565410	5.9	4	4	4	249.78450	1	1.137	636	17
10	1090	339.660784	-8.558875	5.3	4	4	4	249.88686	1	1.137	690	17
11	4005	339.663681	-8.665462	16.4	1	1	4	609.54157	1	1.266	2828	15
11	5002	339.680263	-8.658790	24.6	0	1	4	609.60102	1	1.266	4407	15
11	8001	339.735623	-8.635671	29.5	0	1	4	609.88002	1	1.295	5221	17
11	9013	339.754758	-8.626909	14.6	0	4	4	609.98160	1	1.295	2791	17
12	4018	339.647658	-8.645995	10.2	3	3	4	609.54190	1	1.134	1141	15
12	5028	339.659803	-8.641898	7.8	0	3	3	609.60146	1	1.134	984	15
12	8014	339.701216	-8.625838	15.0	2	2	4	609.88251	1	1.159	1659	17
12	9005	339.715405	-8.619379	16.5	4	4	4	609.98432	1	1.159	2321	17
13	4022	339.672085	-8.528938	7.4	3	3	4	609.53713	1	1.047	778	15
13	5075	339.679506	-8.526589	5.6	4	4	3	609.59736	1	1.047	961	15
13	8016	339.699610	-8.517709	9.7	4	4	4	609.87944	1	1.035	1154	17
13	9025	339.706524	-8.514754	8.5	3	3	4	609.98147	1	1.035	987	17
14	4024	339.761948	-8.551948	6.4	4	4	4	609.53074	1	1.092	866	15
14	5014	339.770892	-8.545951	10.0	4	4	4	609.59120	1	1.092	1137	15
14	9023	339.804980	-8.513935	6.9	0	4	4	609.97516	0	1.092	1209	17
15	8161	339.809759	-8.565357	4.7	0	4	1	609.87345	0	1.234	690	17
15	9064	339.828591	-8.565200	4.7	0	4	0	609.97520	0	1.234	713	17
16	4076	339.695200	-8.541871	5.3	3	3	3	609.53601	1	1.106	652	15
16	5135	339.706170	-8.538451	4.2	4	4	1	609.59578	1	1.106	485	15
16	8056	339.741951	-8.523027	8.6	4	4	4	609.87615	1	1.115	826	17
16	9045	339.754062	-8.517344	4.8	4	4	1	609.97850	1	1.115	730	17
17	4119	339.630591	-8.616134	4.3	4	4	1	609.54245	1	3.715	1609	15
17	5219	339.655302	-8.567826	4.5	4	4	1	609.59977	1	3.715	1523	15
18	4122	339.723015	-8.643114	6.9	4	4	3	609.53682	1	1.149	762	15
18	5051	339.736023	-8.639538	7.0	0	4	4	609.59631	1	1.149	812	15
18	8031	339.776996	-8.625246	8.3	0	3	2	609.87701	1	1.174	870	17
18	9174	339.792203	-8.619354	4.3	0	4	1	609.97887	1	1.174	432	17
19	4137	339.700181	-8.610512	4.1	4	4	1	609.53769	1	1.415	699	15
19	5048	339.721199	-8.604013	6.5	4	4	4	609.59626	1	1.415	930	15
20	8010	339.738208	-8.687407	14.9	0	3	4	609.88123	0	1.727	5686	17
20	9017	339.770672	-8.684256	6.6	0	4	4	609.98219	0	1.727	2001	17

Table 5. Known Asteroids in the 15 June 1996 ISO Field

(IDAS) Asteroid	ID	RA (deg)	DEC (deg)	FD (μ Jy)	SNR	UTC
(1)	3	339.57598	-08.57781	4032	25.1	06 58
1999 AQ23		339.57288	-08.57761			
(1)	1008	339.58899	-08.58097	4339	17.2	09 25
1999 AQ23		339.58596	-08.58042			
(2)	4	339.64707	-08.46325	5543	22.0	06 45
17971 1999 JZ50		339.64713	-08.46247			
(2)	1003	339.67256	-08.45494	5522	24.3	09 11
17971 1999 JZ50		339.67267	-08.45481			

Table 6. Horizons Initial Heliocentric Osculating Elements for Ecliptic and Mean Equinox of J2000.0 and Epoch = 2001-Oct-18.0000000 (TDB), for 1999 AQ23 and 2001-Apr-01.0000000 (TDB), for 17971 1999 JZ50¹

Asteroid	Tp	q	e	AP	Omega	i	H
1999 AQ23	2451507.3543131	2.304351999	0.1217025	97.89149	135.42849	14.72242	13.5
17971 1999 JZ50	2451472.0746345	1.887653106	0.168258407	167.6773526	128.5014528	2.9364673	14.8

¹ Tp = Time of perihelion passage (Julian date), q = Perihelion distance (AU), e = Eccentricity, AP = Argument of perihelion (deg), Omega = Longitude of the ascending node (deg), i = Inclination (deg), H = Absolute visual magnitude (G, the slope parameter, is assumed to be 0.15 for both asteroids). These data were obtained from Horizons on 9 Sep 2001.

Table 7. Aspect Data, Flux, and Derived Diameters and Albedos for Known Asteroids Potentially Associated With IDAS Sources

Asteroid	V mag	H Dist AU	G Dist AU	Phase deg	Flux mJy	D-STM km	p _H -STM	D-NEATM km	p _H -NEATM
1999 AQ23	18.2	2.538	2.053	22.57	4.08 ± 0.15	2.80 ± 0.02	0.90 ± 0.01	3.30 ± 0.02	0.65 ± 0.01
17971 1999 JZ50	18.1	1.892	1.333	31.01	5.57 ± 0.01	1.50 ± 0.01	0.93 ± 0.01	1.73 ± 0.01	0.71 ± 0.01
Below are results assuming the actual H is one full magnitude higher									
1999 AQ23	19.2	2.538	2.053	22.57	4.08 ± 0.15	2.41 ± 0.02	0.48 ± 0.01	2.95 ± 0.02	0.32 ± 0.01
17971 1999 JZ50	19.1	1.892	1.333	31.01	5.57 ± 0.01	1.30 ± 0.01	0.50 ± 0.01	1.54 ± 0.01	0.36 ± 0.01
Below are results assuming the actual H is 0.5 magnitude higher and the Flux a factor of 1.5 greater.									
1999 AQ23	18.7	2.538	2.053	22.57	6.12 ± 0.15	3.00 ± 0.02	0.51 ± 0.01	3.60 ± 0.02	0.34 ± 0.01
17971 1999 JZ50	18.6	1.892	1.333	31.01	8.36 ± 0.01	1.60 ± 0.01	0.52 ± 0.01	1.90 ± 0.01	0.37 ± 0.01

Figures

1	2	3	3	3	3	3	3	3	3	3	3	3	3	3	3	3	2	1
2	4	6	6	6	6	6	6	6	6	6	6	6	6	6	6	6	4	2
3	6	9	9	9	9	9	9	9	9	9	9	9	9	9	9	9	6	3
3	6	9	9	9	9	9	9	9	9	9	9	9	9	9	9	9	6	3
3	6	9	9	9	9	9	9	9	9	9	9	9	9	9	9	9	6	3
3	6	9	9	9	9	9	9	9	9	9	9	9	9	9	9	9	6	3
3	6	9	9	9	9	9	9	9	9	9	9	9	9	9	9	9	6	3
3	6	9	9	9	9	9	9	9	9	9	9	9	9	9	9	9	6	3
3	6	9	9	9	9	9	9	9	9	9	9	9	9	9	9	9	6	3
3	6	9	9	9	9	9	9	9	9	9	9	9	9	9	9	9	6	3
3	6	9	9	9	9	9	9	9	9	9	9	9	9	9	9	9	6	3
3	6	9	9	9	9	9	9	9	9	9	9	9	9	9	9	9	6	3
3	6	9	9	9	9	9	9	9	9	9	9	9	9	9	9	9	6	3
3	6	9	9	9	9	9	9	9	9	9	9	9	9	9	9	9	6	3
3	6	9	9	9	9	9	9	9	9	9	9	9	9	9	9	9	6	3
3	6	9	9	9	9	9	9	9	9	9	9	9	9	9	9	9	6	3
3	6	9	9	9	9	9	9	9	9	9	9	9	9	9	9	9	6	3
2	4	6	6	6	6	6	6	6	6	6	6	6	6	6	6	6	4	2
1	2	3	3	3	3	3	3	3	3	3	3	3	3	3	3	3	2	1

Figure 1. Sample Region Coverage of a 17 x 17 Raster Map. Each 1' x 1' cell shows the total number of 20 second integration sets made on that area.

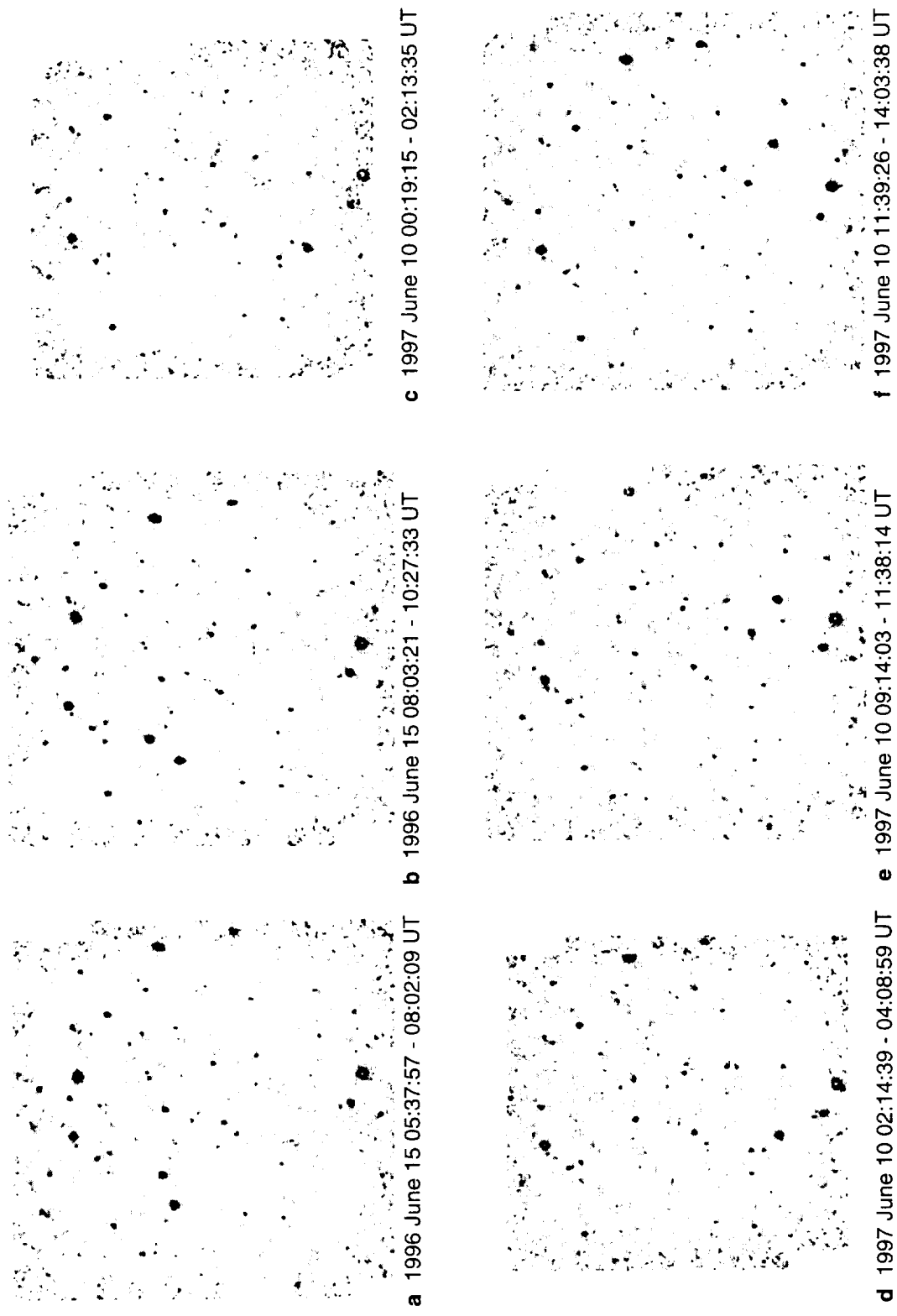
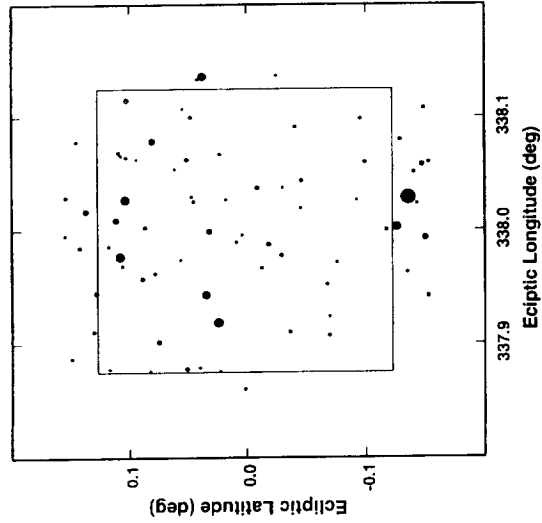
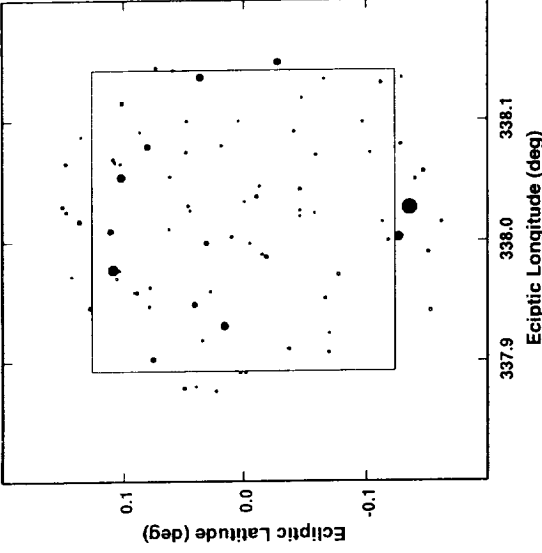


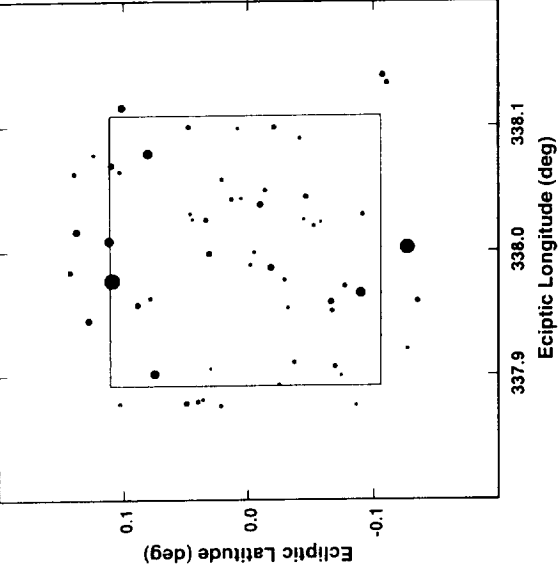
Figure 2. ISOCAM maps in ecliptic coordinates: 1996 June 15 (a, b) and 1997 June 10 (c, d e, f). North ecliptic latitude is up and east ecliptic longitude is to the right. Maps a, b, d, and f are 17x17 rasters while c and e are 15x15 rasters.



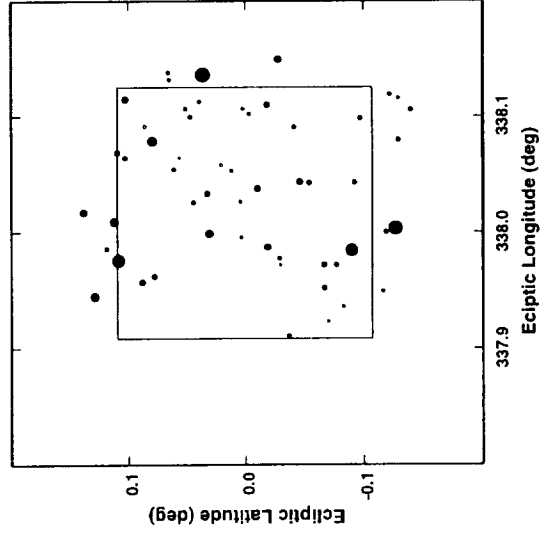
a 1996 June 15 05:37:57 - 08:02:09 UT



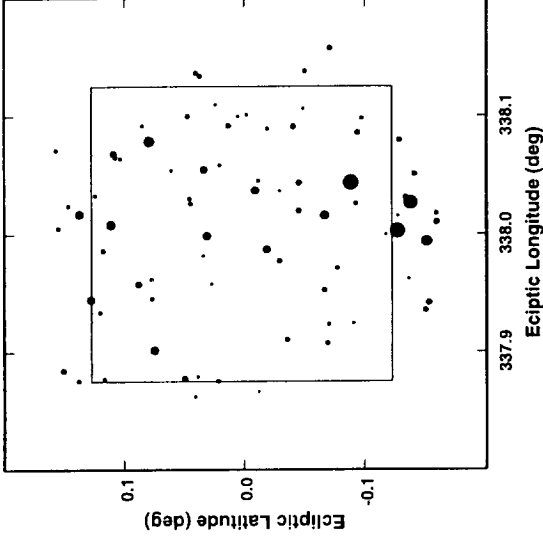
b 1996 June 15 08:03:21 - 10:27:33 UT



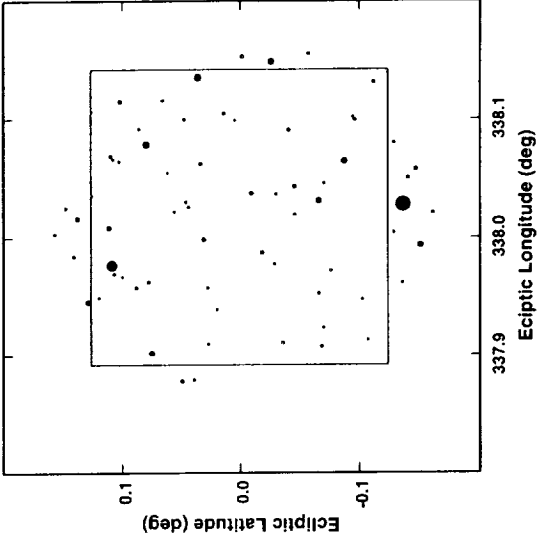
c 1997 June 10 00:19:15 - 02:13:35 UT



d 1997 June 10 02:14:39 - 04:08:59 UT



e 1997 June 10 09:14:03 - 11:38:14 UT



f 1997 June 10 11:39:26 - 14:03:38 UT

Figure 3. Point sources from the ISOCAM maps shown in Figure 2. Squares outline the areas sampled nine times. The point size is proportional to the flux density, which ranges from 0.3 to 10.8 mJy.

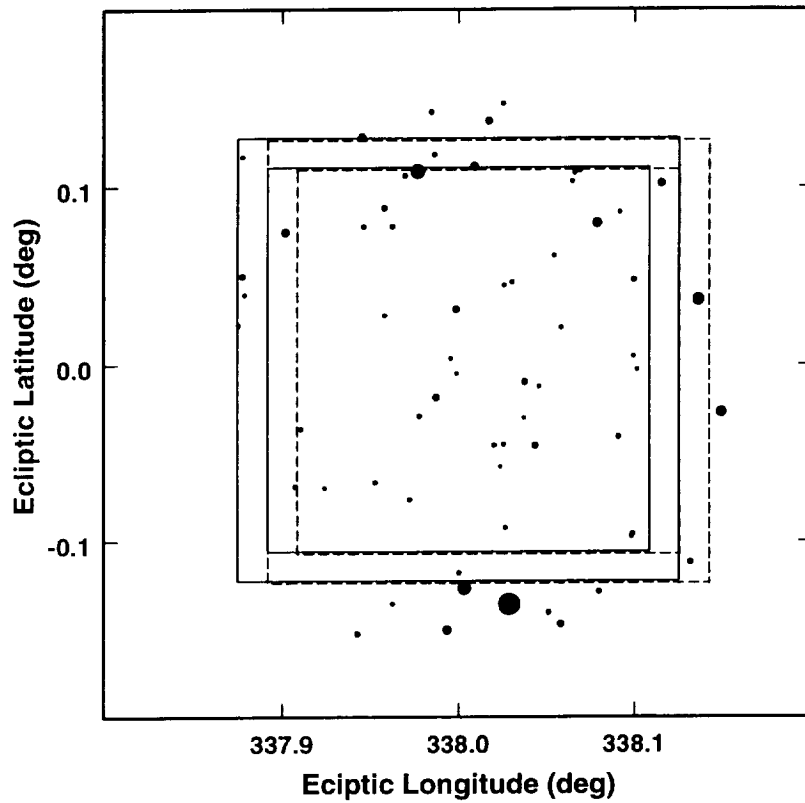


Figure 4. IDAS Inertial Point Sources. Squares outline the areas sampled nine times per map. The inertial sky within the union of the two large squares was sampled 36 times (total integration time 720 sec per map pixel) and that within the two small squares 54 times (total integration time 1,080 sec per map pixel). The point size is proportional to the flux density, which ranges from 0.3 to 10.8 mJy.

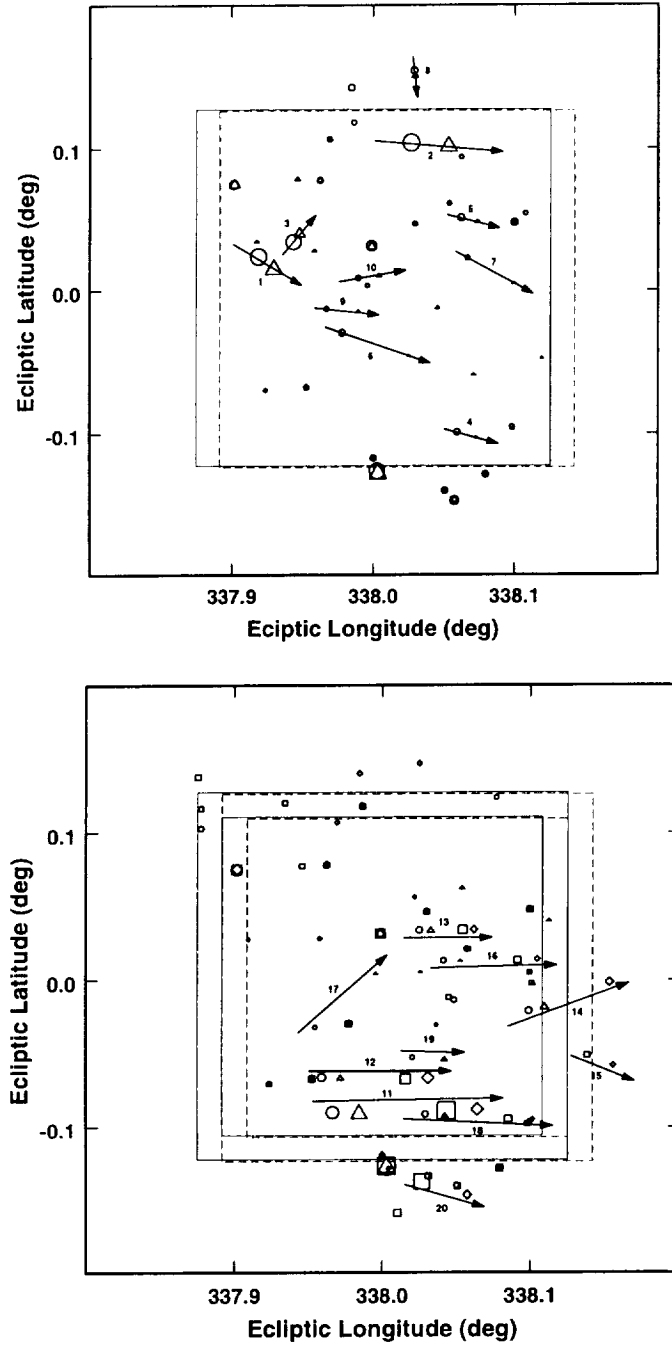


Figure 5. IDAS Non-inertial Point Sources, i.e., all sources from Fig 3 not plotted in Fig 4. Sources from the 1996 field are plotted in the top panel and those from the 1997 field in the bottom panel. Squares outline the areas sampled nine times per map. The point size is proportional to the flux density, which ranges from 0.4 to 4.3 mJy. Circles indicate sources extracted from Maps 1 (top) or 3 (bottom), triangles those from Maps 2 (top) or 4 (bottom), squares those from Map 5, and diamonds those from Map 6.

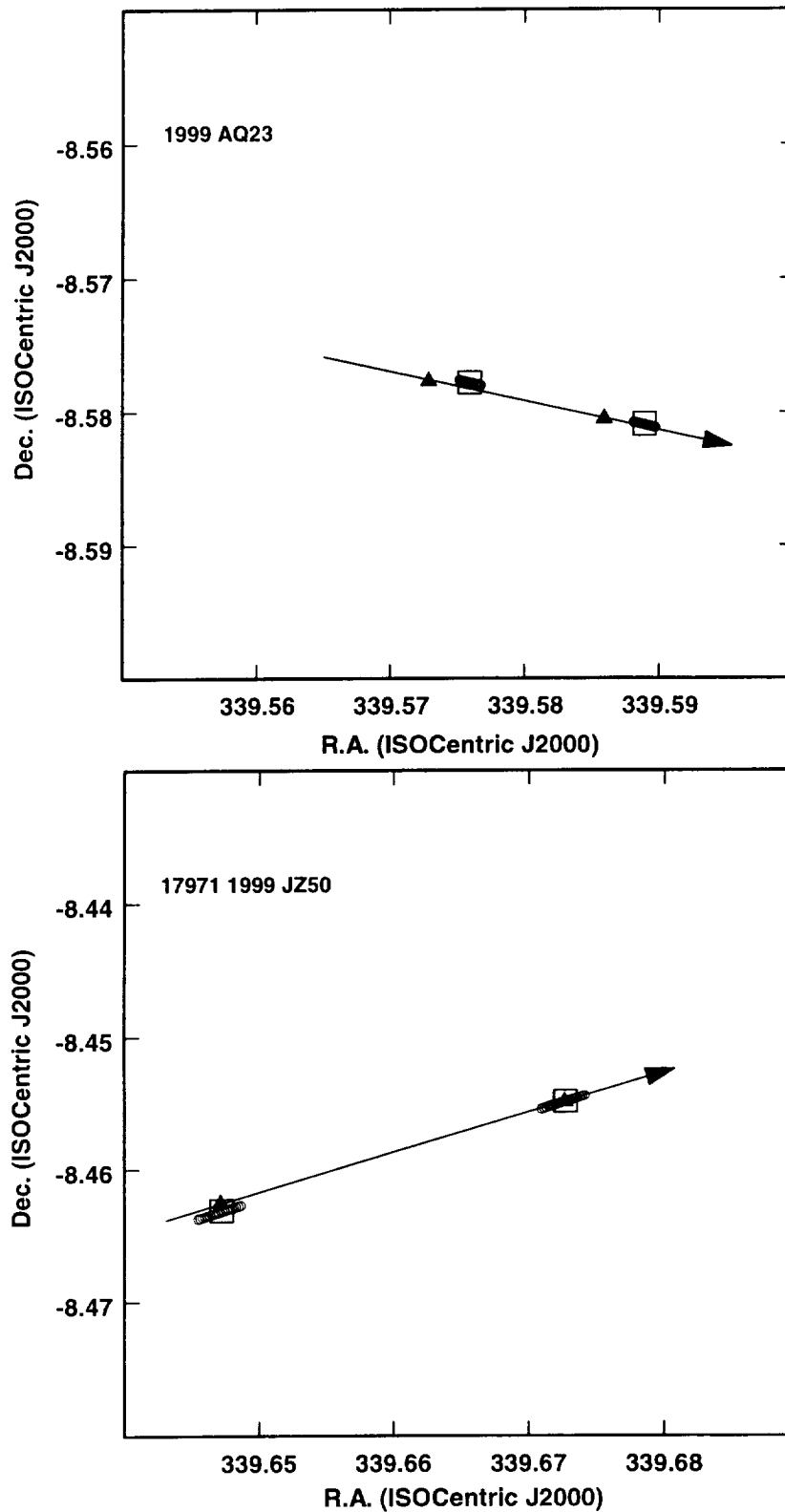


Figure 6. Observed (circles) versus predicted (triangles) positions for two bright known asteroids in the 1996 ISO map. Each graph is 3' on a side, the approximate size of the ISOCAM array. The small squares centered on the observed position are 6" on a side, the approximate size of the ISOCAM PFOV used.

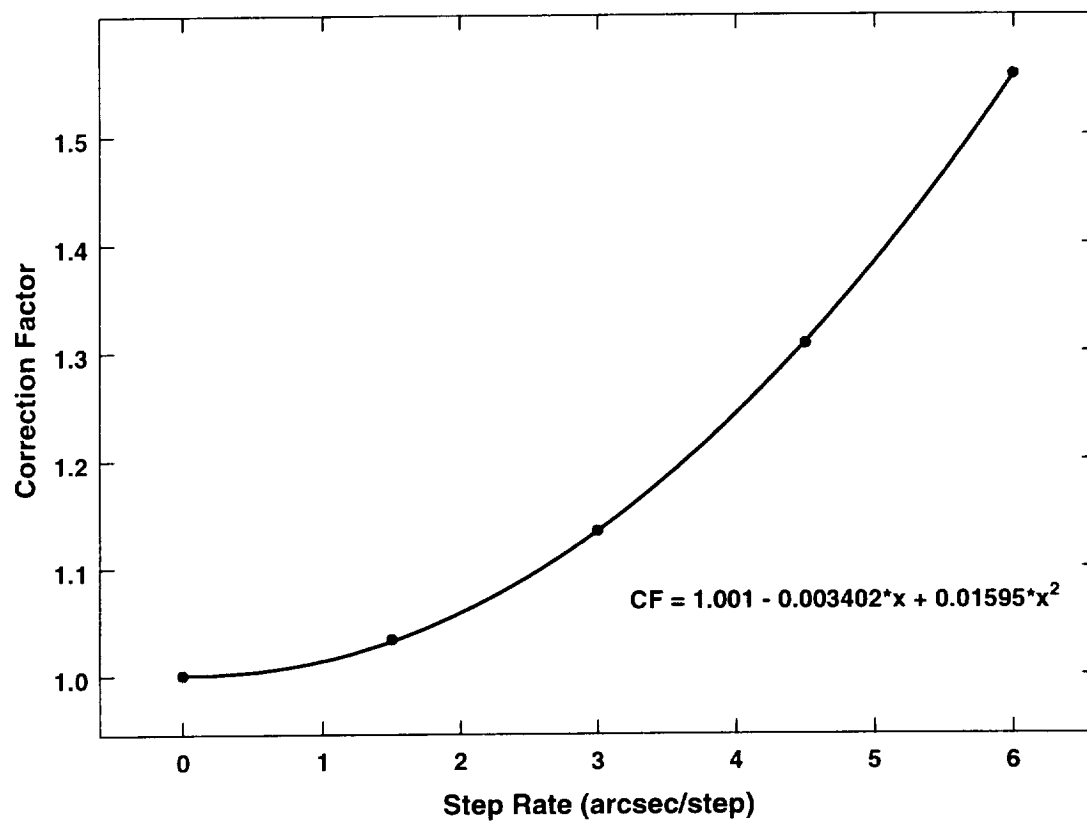


Figure 7. Moving source flux correction.

REPORT DOCUMENTATION PAGE		Form Approved OMB NO. 0704.0188	
Public reporting burden for this collection of information is estimated to average 1 hour per response, including the time for reviewing instructions, searching existing data sources, gathering and maintaining the data needed, and completing and reviewing the collection of information. Send comments regarding this burden estimate or any other aspect of the collection of information, including suggestions for reducing this burden, to Washington Headquarters Services, Directorate for Information Operations and Reports, 1215 Jefferson Davis Highway, suite 1204, Arlington, VA 22202-4302, and to the Office of Management and Budget, Paperwork Reduction Project (0704-0188), Washington, DC 20503.			
1. AGENCY USE ONLY (Leave Blank)	2. REPORT DATE 09/21/2001	3. REPORT TYPE AND DATES COVERED NASA Formal Report Series Final Report	
4. TITLE AND SUBTITLE Asteroid Size-Frequency Distribution		5. FUNDING NUMBERS NAS5-97215	
6. AUTHOR(s) Edward F. Tedesco		8. PERFORMING ORGANIZATION REPORT NUMBER ISO_FR_25	
7. PERFORMING ORGANIZATION NAME(S) AND ADDRESS(ES) TerraSystems, Inc. 2800 Woodlawn Drive, Suite 264 Honolulu, HI 96822			
9. SPONSORING/MONITORING AGENCY NAME(S) AND ADDRESS(ES) NASA ADP Office Goddard Space Flight Center Greenbelt, MD 20771-0001		10. SPONSORING/MONITORING AGENCY REPORT NUMBER	
11. SUPPLEMENTARY NOTES			
12a. DISTRIBUTION/AVAILABILITY STATEMENT Unlimited		12b. DISTRIBUTION CODE	
ABSTRACT (Maximum 200 words) A total of six deep exposures (using AOT CAM01 with a 6" PFOV) through the ISOCAM LW10 filter (IRAS Band 1, i.e., 12 μ m) were obtained on a ~15 arcminute square field centered on the ecliptic plane. Point sources were extracted using the technique described by Desert, et al. (1999, A&A 342, 363). Two known asteroids appear in these frames and 20 sources moving with velocities appropriate for main belt asteroids are present. Most of the asteroids detected have flux densities less than 1 mJy, i.e., between 150 and 350 times fainter than any of the asteroids observed by IRAS (Tedesco, et al., 2002a, Astron J., submitted). These data provide the first direct measurement of the 12 μ m sky-plane density for asteroids on the ecliptic equator. The median zodiacal foreground, as measured by ISOCAM during this survey, is found to be 22.1 ± 1.5 mJy per pixel, i.e., 26.2 ± 1.7 MJy/sr. The results presented here imply that the actual number of kilometer-sized asteroids is significantly greater than previously believed and in reasonable agreement with the Statistical Asteroid Model (Tedesco, et al., 2002b, Astron J., to be submitted.).			
14. SUBJECT TERMS Asteroids Infrared			15. NUMBER OF PAGES
			16. PRICE CODE
17. SECURITY CLASSIF. OF REPORT UNCLASSIFIED	18. SECURITY CLASSIF. OF THIS PAGE UNCLASSIFIED	19. SECURITY CLASSIF. OF ABSTRACT UNCLASSIFIED	20. LIMITATION OF ABSTRACT Unlimited

Standard Form 298 (Rev. 2-89)
Prescribed by ANSI Std. Z39-18
298-102

UNCLASSIFIED

 SECURITY CLASSIFICATION OF THIS PAGE